

Thermal Convection Analysis in a Rotating Shell by Parallel FEM - Development of a Thermal-Hydraulic Subsystem of GeoFEM -

Hiroaki Matsui ⁽¹⁾ and Hiroshi Okuda ⁽²⁾

(1) Department of Research for Computational Earth Science, Research Organization for Information Science & Technology (RIST), Tokyo, JAPAN (e-mail: matsui@tokyo.rist.or.jp, Phone: +81-3-3436-5271, fax: +81-3436-5274, (2) Department of Quantum Engineering and System Science, The University of Tokyo, Tokyo, Japan (e-mail: okuda@q.t.u-tokyo.ac.jp, phone: +81-3-5841-7426, fax: +81-3813-3455)

Abstract

The purpose of this paper is to propose a method for the numerical simulation of thermally driven convection in a rotating spherical shell modeled on the Earth's outer core using the GeoFEM Thermal-Hydraulic subsystem, which provides a parallel FEM platform. This simulation is designed to assist in the understanding of the origin of the geomagnetic field and the dynamics of the fluid in the Earth's outer core. A three-dimensional and time dependent process of a Boussinesq fluid in a rotating spherical shell is solved under the effects of self gravity and the Coriolis force. A tri-linear hexahedral element is used for the spatial distribution. A total of 1.26×10^5 nodes were used on the spherical shell, and the finite element mesh divided into 32 domains for parallel computation. The 2nd-order Adams-Bashforth scheme was used for the time integration of temperature and velocity. To satisfy mass conservation, a parallel iterative solver given by GeoFEM was used to solve for the pressure and correction of the velocity fields, and the simulation was performed over 10^5 steps using 4 nodes of a Hitachi SR8000. To verify the proposed simulation code, results of the simulation are compared with analysis by the spectral method. The results show that the outline of convection is approximately equal; that is, three pairs of convection columns are formed, and these columns propagate westward in a quasi-steady state. However, the magnitude of kinetic energy averaged over the shell is approximately 93% of that by the spectral method, and the drift frequency of the columns in the GeoFEM simulation is larger than that by the spectral method.

1. Introduction

It has been widely accepted that the geomagnetic field is generated by motion of an electrically conductive fluid in the Earth's outer core. This process is referred to as a geodynamo process. The motion of fluid is strongly influenced by the Lorentz force and the Coriolis force which, in a co-rotating frame, is given by, $-2\rho\Omega \times \mathbf{v}$, where ρ , Ω , and \mathbf{v} are the density of the fluid, angular velocity of the Earth's rotation, and velocity of the fluid, respectively. Furthermore, the dynamo process is not only a complicated nonlinear system, but also requires three-dimensional and time dependent treatment for direct simulation. In the last five years, investigation of the generation processes of the Earth and planetary magnetic fields has entered into a new stage; several magnetohydrodynamic (MHD) simulations in a rotating spherical shell have been used to represent some of the basic characteristics of the

field (Glatzmaier and Roberts, 1995a[9], 19995b[10] and Kageyama et.al., 1995[13]). Following these studies, many studies of the geodynamo simulation represent strong and dipole like magnetic fields by which the geomagnetic field is characterized (Kuang and Bloxham, 1997[14], 1999[15]; Christensen, 1999[5], Sakuraba (1999)[19]). However, most of these simulations applied a spherical harmonics expansion in the azimuthal and elevation directions, because high spectral accuracy is obtained in this method, singularity of physical values is maintained at the poles, and magnetic fields are easily connected to the potential field on the boundaries. Kageyama et. al. (1995)[13] applied the finite difference method (FDM). However, they considered a compressible gas for a model of the fluid and applied a different magnetic boundary condition at the outer boundary of the shell to the condition estimated at the Earth's Core-Mantle boundary. Fornberg and Merill (1997) [6] carried out a simulation of fluid motion on a sphere by FDM and pseudospectral method and compared the results, and concluded that the pseudospectral methods are more cost-effective than the FDM.

These previous studies successfully modeled the basic processes of the geodynamo, but dimensionless numbers in these simulations were significantly different to those estimated in the outer core; for example, the Taylor number and the Rayleigh number are estimated to be 10^{30} using molecular diffusivity. To carry out simulations with such large Taylor and Rayleigh numbers, a high spatial resolution is required. Thus, large scale simulations of the motion in a rotating spherical shell on massively parallel computers are required. The spectral harmonics expansion, which is the general scheme for the geodynamo simulation is, however, not suitable for massively parallel computation because a significant number of global calculations are required in the process; that is, a spectral harmonics transform is required to solve nonlinear terms. Lesur and Gubbins(1999)[17] showed a fast algorithm for the spherical transformation, but a global operation is also required in this method. Kuang and Bloxham (1997[14], 1999[15]) divided the spherical shell in the radial direction for parallel computation, but the number of processes depends on the number of radial grid points in this method. There are many other schemes for the simulation of fluid motion such as the finite volume method(FVM), and finite element method(FEM). These schemes are more suitable for parallel computation because they consist of local operations. Comparing with FDM, FVM and FEM are more suitable for the simulation of a fluid in a spherical shell because singularity of physical values at poles is satisfied. Schmalzl and Hansen (2000) [20] used FVM to carry out a dynamo simulation in a cartesian domain because it requires less memory and computational power than FEM. However, it is possible to set any unstructured mesh and domain decomposition pattern in FEM. The present authors are developing a simulation code for a MHD simulation in a rotating spherical shell to assist in the understanding of the geodynamo process and dynamics of a fluid in the shell using GeoFEM [8], which gives a parallel FEM platform for solid Earth simulation. GeoFEM is being developed as a part of a five-year project called the Earth Simulator project, that was initiated by the Science and Technology Agency of Japan (STA) in 1997. The aim of this project is the development of hardware and softwares for earth science simulations. We have developed a simulation code for thermal convection in a rotating flame without a magnetic field and carried out numerical simulations of the thermal convection in a rotating spherical shell. The results are compared with simulation results by spectral harmonics expansion. In this study, we compare the two sets of results to verify the proposal approach. The paper consists of the following sections: In section 2, we describe the simulation model and methods. Results of the simulations are given in Section 3. In Section 4, a discussion of the results is presented and conclusions are made in Section 5.

2. Simulation Model and Methods

Proposed Model

Consider a rotating spherical shell modeled on the Earth's outer core as given in Fig.1. The

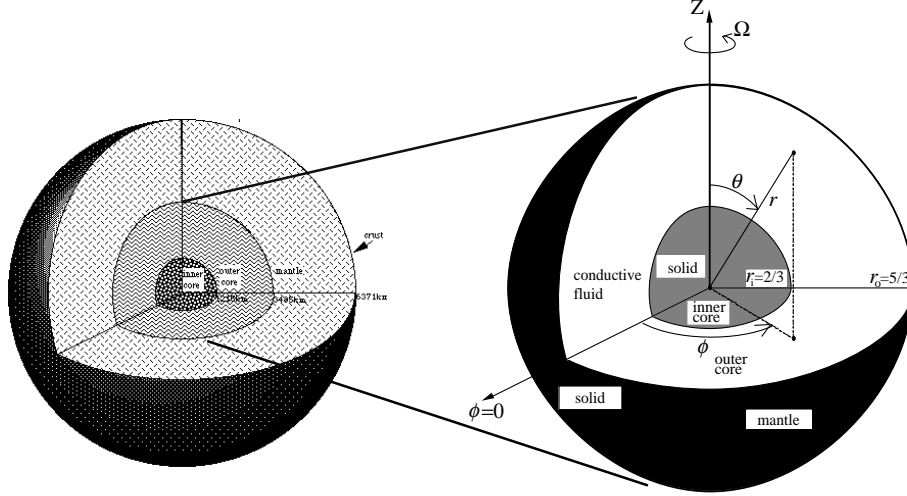


Figure 1: Rotating spherical shell modeled on the Earth's outer core. A sketch of the interior of the Earth is given in the left panel, and the rotating spherical shell model is given in the right panel.

ratio of the inner boundary to the outer boundary of the spherical shell is set to 0.4 while the ratio of the radius of the inner core boundary (ICB) to that of the outer core boundary (CMB) is approximately 0.35. The shell is filled with a Boussinesq fluid and rotates with a uniform angular velocity Ω . The fluid has a constant thermal diffusivity κ , kinetic viscosity ν , and thermal expansion coefficient α . We assume that the inner core co-rotates with the mantle to simplify the model. The motion of a fluid in a rotating flame is described by the mass conservation, the momentum equation (Navier-Stokes equation) with the Boussinesq approximation and the Coriolis term, and the thermal diffusion equations; that is,

$$\operatorname{div} \mathbf{v} = 0, \quad (1)$$

$$\frac{\partial \mathbf{v}}{\partial t} + (\mathbf{v} \cdot \nabla) \mathbf{v} = -\nabla P + P_r \nabla^2 \mathbf{v} - P_r \sqrt{T_a} (\Omega \times \mathbf{v}) + P_r R_a \Theta \mathbf{r}, \quad (2)$$

$$\frac{\partial \Theta}{\partial t} + (\mathbf{v} \cdot \nabla) (\Theta + T_0) = \nabla^2 \Theta, \quad (3)$$

$$T = \Theta + T_0, \text{ and} \quad (4)$$

$$T_0 = \frac{r_i r_o - r_i r}{r (r_o - r_i)}, \quad (5)$$

where, \mathbf{v} , P , Ω , \mathbf{r} , Θ , T_0 , r_o , and r_i are the velocity, modified pressure, vector of the Earth's rotation, position vector, perturbation of temperature, reference temperature, radius of the outer boundary of the shell, and radius of the inner boundary of the shell, respectively. To obtain above normalized equations, a shell width $L = r_o - r_i$ and thermal diffusion time L^2/κ were selected as the length scale and time scale, respectively. There are three dimensionless numbers in the above equations; that is, the Prandtl number P_r , the Rayleigh number R_a , and the Taylor number T_a . These numbers are given by,

$$P_r = \frac{\nu}{\kappa}, \quad (6)$$

$$R_a = \frac{g\alpha\Delta TL^3}{\kappa\nu}, \text{ and} \quad (7)$$

$$T_a = \left(\frac{2\Omega L^2}{\nu} \right)^2, \quad (8)$$

where ν , κ , α , ΔT , and g are the kinetic viscosity, thermal diffusivity, thermal expansion ratio, and difference of temperature between the inner and outer boundaries of the shell, respectively. The Taylor number and Rayleigh number in the Earth's outer core are estimated to be $T_a = 10^{30}$ and $R_a = 6 \times 10^{30}$ with the molecular viscosities (Gubbins, 1987[11]). Even if we consider turbulent viscosities, these dimensionless numbers remain greater than 10^{10} . However, these estimated values can not be used directly because of limitation of computational power. Therefore, let the Prandtl number be 1, the Taylor number be 2.5×10^5 , and the Rayleigh number be $1.5 \times 10^4 = 1.8R_{ac}$, where R_{ac} is the critical Rayleigh number.

The boundary conditions exert a significant influence on the motion of the fluid. Rigid boundary conditions were selected for the velocity and a fixed temperature for the temperature boundary condition at both boundaries; that is,

$$\mathbf{v} = 0 \quad \text{at } r = r_o, r_i, \quad (9)$$

$$T = 1 \quad \text{at } r = r_i, \text{ and} \quad (10)$$

$$T = 0 \quad \text{at } r = r_o. \quad (11)$$

Simulation by the GeoFEM methods

The simulation code is based on the GeoFEM Thermal-Hydraulic subsystem, which was designed for numerical simulation of thermally driven convection by parallel FEM. In this subsystem, the basic equations eqs. (1) - (3) for the fluid are solved three dimensionally and time dependently. The spherical shell is divided into tri-linear hexahedron elements, and the temperature, velocity, and pressure are defined at each node and interpolated by tri-linear function in each hexahedron element. For the time integration, the fractional step scheme and Adams-Bashforth scheme are applied to obtain an accurate estimation of the Coriolis term. The simulation process is given by the following equations;

$$\bar{M}_{\alpha\beta}\Theta_{\beta}^{n+1} = \bar{M}_{\alpha\beta}\Theta_{\beta}^n + \Delta t \left(\frac{3}{2}F_T^n - \frac{1}{2}F_T^{n-1} \right), \quad (12)$$

$$\bar{M}_{\alpha\beta}\tilde{v}_{i\beta} = \bar{M}_{\alpha\beta}v_{i\beta}^n + \Delta t \left(\frac{3}{2}F_{vi}^n - \frac{1}{2}F_{vi}^{n-1} \right), \quad (13)$$

$$\frac{1}{\Delta t} (-L_{\alpha\beta} + S_{\alpha\beta}) \Phi_{\beta} = H_{\alpha\beta}^i \tilde{v}_{i\beta}, \quad (14)$$

$$P_{\alpha}^{n+1} = \frac{1}{\Delta t} \Phi_{\alpha}, \text{ and} \quad (15)$$

$$\bar{M}_{\alpha\beta}v_{i\beta}^{n+1} = \bar{M}_{\alpha\beta}\tilde{v}_{i\beta} + H_{\alpha\beta}^i \Phi_{\beta}, \quad (16)$$

where the diffusion, inertia, buoyancy, and Coriolis terms are given by,

$$F_T^n = \left\{ (-L_{\alpha\beta} + S_{\alpha\beta}) \Theta_{\beta}^n - H_{\alpha\beta}^j v_{ej}^n (\Theta_{\beta}^n + T_{0\beta}) \right\}, \text{ and} \quad (17)$$

$$F_{vi}^n = \left\{ P_r (-L_{\alpha\beta} + S_{\alpha\beta}) v_{i\beta}^n - H_{\alpha\beta}^j v_{ej}^n v_{i\beta}^n \right. \\ \left. - P_r T_a^{1/2} e_{ijk} M_{\alpha\beta} \Omega_{ja} v_{k\beta} - P_r R_a M_{\alpha\beta} \Theta_{\beta}^{n+1} g_i \right\}. \quad (18)$$

In above equations, e_{ijk} is the permutation symbol, and v_{ei} is velocity averaged over each element where,

$$v_{ei} = \sum_{\alpha=1}^8 v_{i\alpha} \frac{1}{V_e} \int_{\Omega_e} N_\alpha dV. \quad (19)$$

Each component of matrices $M_{\alpha\beta}$, $\bar{M}_{\alpha\beta}$, $L_{\alpha\beta}^i$, $H_{\alpha\beta}^i$, $S_{\alpha\beta}^i$ in eqs.(12)-(17) are described by the following integrations:

$$M_{\alpha\beta} = \int_{\Omega_e} \tilde{N}_\alpha N_\beta dV, \quad (20)$$

$$\bar{M}_{\alpha\beta} = \left[\sum_{\beta} M_{\alpha\beta} \right] \delta_{\alpha\beta}, \quad (21)$$

$$L_{\alpha\beta} = \int_{\Omega_e} \frac{\partial N_\alpha}{\partial x_i} \frac{\partial N_\beta}{\partial x_i} dV, \quad (22)$$

$$H_{\alpha\beta}^i = \int_{\Omega_e} \tilde{N}_\alpha \frac{\partial N_\beta}{\partial x_i} dV, \text{ and} \quad (23)$$

$$S_{\alpha\beta} = \oint_{\Omega_e} \tilde{N}_\alpha \frac{\partial N_\beta}{\partial x_i} n_i dS, \quad (24)$$

where, N_α is a tri-linear shape function and the upwinded shape function \tilde{N}_α is defined as,

$$\tilde{N}_\alpha = N_\alpha + \frac{\Delta t}{2} v_{ej} \frac{\partial N_\alpha}{\partial x_j}. \quad (25)$$

First, the temperature is solved using eq.(12) with eq.(18). Then, to obtain a predictor of the velocity \tilde{v}_i eq.(13) with eq.(17) are solved. To satisfy the mass conservation low, divergence of the predictor is calculated and Poisson equation eq.(14) is solved by the parallel iterative solver of GeoFEM. Then pressure p^{n+1} and velocity v_i^{n+1} are solved by eqs.(15) and (16).

The advantage of FEM is that the operations given in eqs(12), (13), (15), and (16) are local operations; that is, the values at each node are solved by neighboring nodes. The finite element mesh is divided into local domains in GeoFEM, and each local data structure is node based with overlapping elements (Nakajima, 1999[18]). Thus, eqs(12), (13), (15), and (16) are solved in separate processor. A global operation is only required to solve the Poisson equation Eq.(14). The iteration solver in GeoFEM is used for this operation, because an iterative solver with preconditioning is one of the most powerful methods for parallel computing (Nakajima, 1999[18]). Because the grid data have communication tables and routines for communication are concentrated in the solver subroutine, it is possible to develop a code with few special treatments for parallel computation.

Grid Pattern

The spherical shell is divided into tri-linear hexahedral finite elements. A grid pattern is set on a sphere to be based on an icosahedron following Baumgardner and Frederickson (1984[1]) and Stuhne and Peltier (1996[21], 1999[22]); the grid pattern is obtained by three levels of refinement from an icosahedron. To obtain a hexahedral element, each triangle is divided into three quadrilaterals. Finally, this mesh is stacked in the radial direction. The spherical shell is divided into 33 layers including both boundaries in the radial direction and 3842 nodes are set on each sphere surface. Distances between nodes are approximately 70 km in the radial direction and 3 degrees in the longitudinal direction at the equator. The domain

decomposition method has been applied in GeoFEM for parallel computation, and single program multiple data. The finite element mesh is divided into 32 domains by Recursive Coordinate Bisection(RCB); that is, the mesh is divided by planes that are parallel with respect to the x , y , and z planes and to balance the number of nodes in each domain. The grid pattern of the spherical shell is given in Fig.2. This partitioning is carried out by the partitioner in GeoFEM that generates a communication table for iterative solver at the same time.

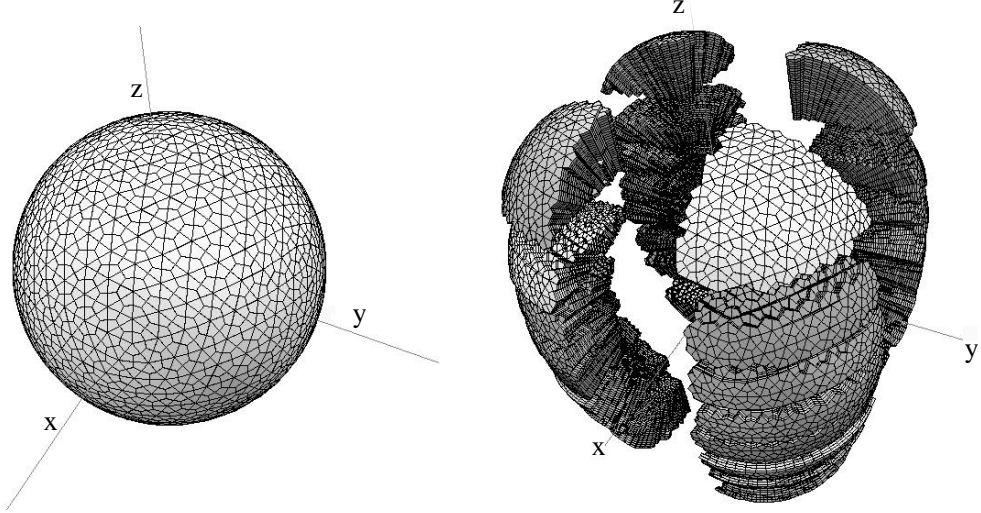


Figure 2: Grid pattern for the rotating spherical shell. The grid pattern for entire spherical shell is given in the left panel, and distributed grid pattern for parallel computation is given in the right panel.

Simulation by the spectral method

To verify the results of the simulation by GeoFEM, the same simulation was carried out by the spectral method. In this case, the simulation scheme is based after Frazer (1974[7]), Honkura et. al. (1992[12]), and Matsui (1999[16]). It is well established that arbitrary solenoidal vector fields can be separated into poloidal and toroidal components (Bullard, 1954[2]; Chandrasekhar, 1961[4]). The velocity field is solenoidal because the Boussinesq approximation is applied in the present study. Scalar functions of the poloidal velocity V_S and toroidal velocity V_T and temperature perturbation Θ are expanded into the spherical harmonics; that is,

$$\mathbf{v} = \text{rot rot } (V_T \mathbf{r}) + \text{rot } (V_T \mathbf{r}) \quad (26)$$

$$V_S(\mathbf{r}, t) = \sum_{l=1}^L \sum_{m=-l}^l V_{Sl}{}^m(r, t) Y_l^m(\theta, \phi) \quad (27)$$

$$V_T(\mathbf{r}, t) = \sum_{l=1}^L \sum_{m=-l}^l V_{Tl}{}^m(r, t) Y_l^m(\theta, \phi) \quad (28)$$

$$\Theta(\mathbf{r}, t) = \sum_{l=0}^L \sum_{m=-l}^l \Theta_l{}^m(r, t) Y_l^m(\theta, \phi) \quad (29)$$

where, $Y_l^m(\theta, \phi)$ and L are the spherical harmonics and truncation level, respectively. The coefficients of the harmonics V_{Sl}^m , V_{Tl}^m , and Θ_l^m are solved. To find a solution in the radial direction, the 2nd order finite difference method is applied. In this case, The heat conduction equation and vorticity equation for the poloidal and toroidal component of the vorticity are solved. The poloidal velocity is obtained by the toroidal vorticity using the Poisson equation. To solve the time evolution, the Crank-Nicolson scheme is adopted for the diffusion terms and 2nd-order Adams-Bashforth scheme for solving the other terms. It is noted that the inertia terms and the Coriolis term are solved by the coefficients of the spherical harmonics. Because the amount of computation increases $O(L^5)$ order in this scheme, it is difficult to set the truncation level to be significantly large. In this study, the truncation level of the spherical harmonics is set to be 18 degrees with 64 equally spaced grid points in the radial direction.

The simulations were performed on the following computers; the simulation by GeoFEM was performed on 4 nodes of a Hitachi SR8000 and the spectral method was performed on 16 processors of an NEC SX-4.

3. Simulation Results

Three sections of the results of the simulation by GeoFEM were compared with that by the spectral method; that is, i) characteristics of the convection pattern, ii) kinetic energy and z-component of the angular momentum averaged over the spherical shell, and iii) time variation of the convection pattern.

Convection pattern

After Busse (1970[3]), many analytical studies and numerical simulations have demonstrated that columnar convection that is parallel with respect to the rotation axis is formed outside of the tangential cylinder, which is an imaginary cylinder attached to the inner boundary of the shell at the equator, in the case of thermally driven convection in a rotating spherical shell. To show the characteristics of the convection pattern in a quasi-steady state, an isosurface of $P = 1000$ and $P = -1000$ and a contour map of the z-component of vorticity $\omega_z = \text{rot } \boldsymbol{\omega} \hat{z}$ in a cross section at $z = 0.35$ are shown in Fig.3. In the simulation, three pairs of convection columns that are parallel with respect to the rotation axis are formed. As shown in Fig.3, low pressure convection columns have a positive z-component of vorticity and vice versa. In the upper panels of Fig.4, the intensities of the z-component of vorticity and of the velocity at the cross section $z = 0.35$ are given. In the convection columns, the z-component of the velocity and vorticity are in opposite directions; i.e., the clockwise vortices demonstrate poleward flow, while the counterclockwise vortices demonstrate equatorward flow. These structures of the convection are characterized as helical flows. To verify that the simulation works correctly, the convection pattern is compared with that for the case by the spherical harmonics expansion. The z-component of vorticity and velocity at the same cross section are shown in the lower panels of Fig.4. As can be seen, the convection patterns are approximately equal except for position of each convection column. The intensity of the velocity in the case of GeoFEM is, however, smaller than that by the spectral method. This difference is also seen in the magnitude of the kinetic energy averaged over the spherical shell.

Isosurface: Pressure

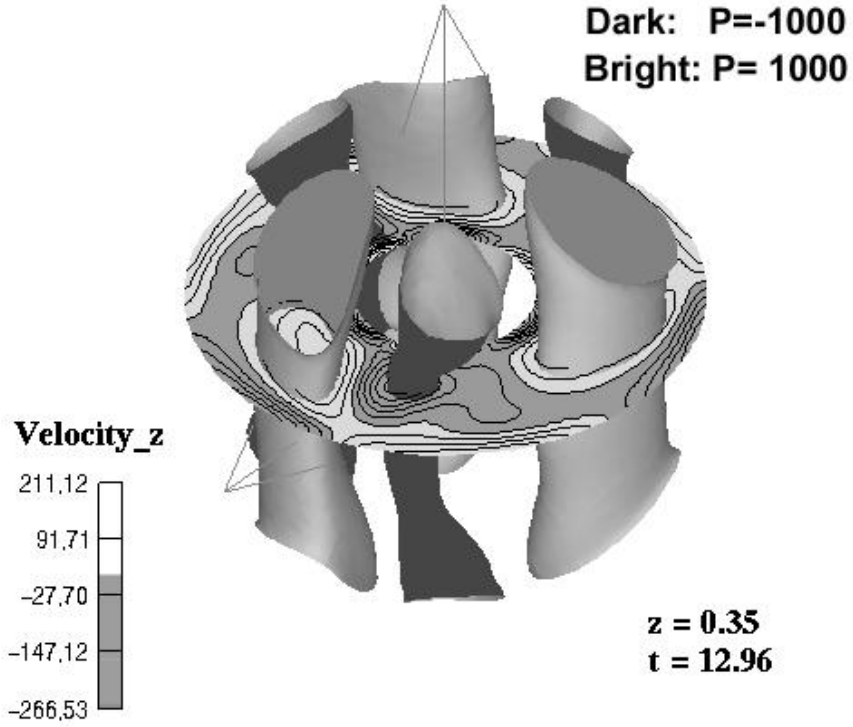


Figure 3: Convection pattern at $t = 12.96$ for the simulation by GeoFEM. Pressure is shown as isosurfaces of $P = -1000$ (dark surface) and $P = 1000$ (bright surface). Intensity of the z-component of vorticity at cross section $z = 0.35$ is given by the contour map. Regions with a negative vorticity are filled dark gray in the contour map.

Averaged kinetic energy and angular momentum

The time evolution of kinetic energy averaged over the spherical shell, which is defined by $\frac{1}{V} \int \frac{1}{2} v^2 dV$, is given in Fig.5. Comparing between the two simulations, differences are observed when $t < 7$. After $t = 11$, however, the behaviors become quite similar. The difference in the initial stages is caused by the difference in the initial temperature in the two cases; that is, in the case of GeoFEM, the initial temperature was set to $T = 1$ on the inner boundary and to $T = 0$ on the other region, while a small temperature perturbation was given in the all mode of the spherical harmonics as the initial temperature for the case by the spectral method. After $t = 11$, the kinetic energy in both cases shows similar changes because the effects of the initial temperature are negligible. The magnitude of the kinetic energy was, however, different for the two cases. The averaged kinetic energy and z-component of the angular momentum $\frac{1}{V} \int (\mathbf{r} \times \mathbf{v}) dV$ at a quasi-steady state are given in Table 1. At $t > 11$, the magnitude of the kinetic energy for the case by GeoFEM was approximately 93% that of the case by the spectral method. Conversely, the z-component of angular momentum averaged over the shell was larger than that by the spectral method. These results suggest that details of convection patterns also differ.

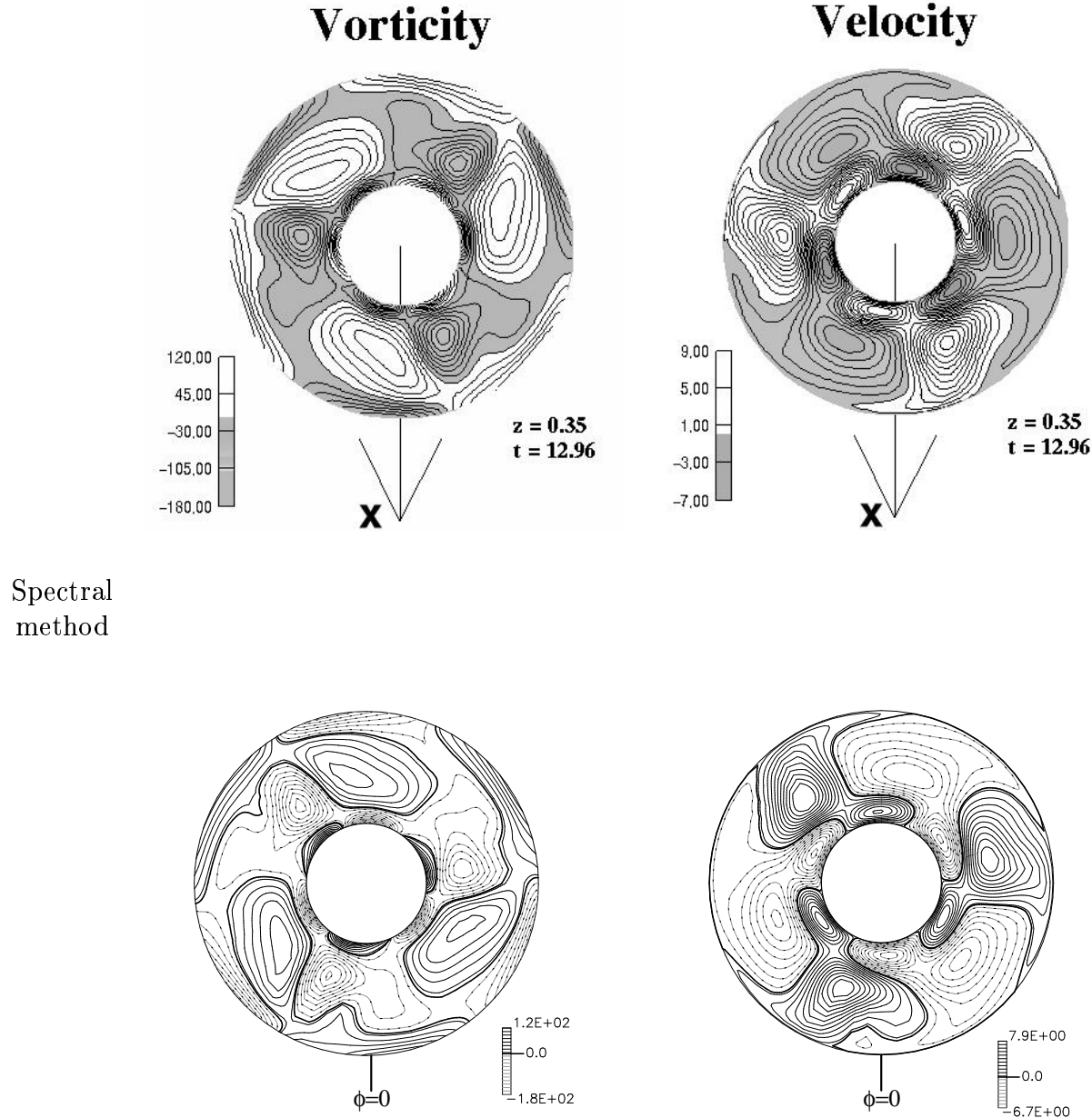


Figure 4: Intensity of the z-component of vorticity (left panels) and velocity (right panels) at cross section $z = 0.34$ in a quasi-steady state. The results for the simulation by GeoFEM at $t = 12.96$ are given in left panels, and the results for the simulation by the spectral method at $t = 12.0$ are given in the right panels. The vorticity range is from -180.0 to 120.0 for both cases, and that of the velocity is from -6.7 to 7.9 for the case by the spectral method and from -7.0 to 9.0 for the case by GeoFEM.

Time variation of convection patterns

As many simulation results have demonstrated, convection patterns propagate in the longitudinal directions as described by

$$(\mathbf{v}, \Theta) = \mathbf{f}(r, \theta, \phi - \omega t), \quad (30)$$

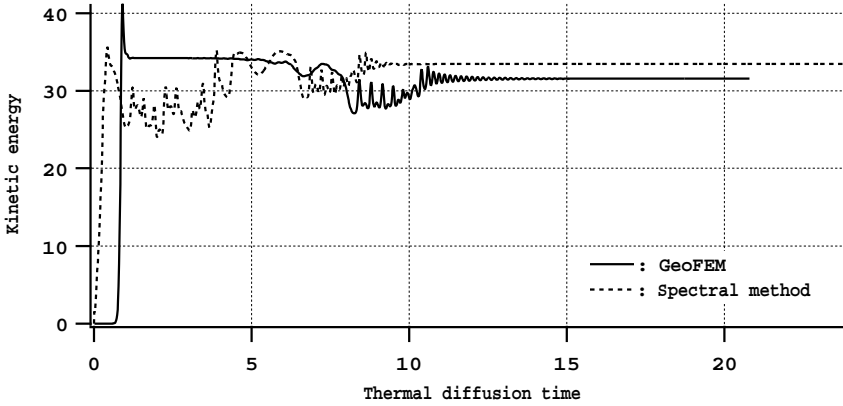


Figure 5: Time evolution of kinetic energy averaged over the spherical shell.

	GeoFEM	Spectral method
Kinetic energy	31.6	33.5
Angular momentum	-0.919	-0.849
drift frequency	-1.88	-1.62

Table 1: Kinetic energy and angular momentum averaged over the spherical shell and drift angular frequency of the convection pattern at $t = 18.0$. A positive drift angular frequency is defined as eastward propagation.

where ω is the drift angular frequency. To investigate variations of the convection patterns and the drift frequency, the radial velocity at the mid-depth of the shell and the equatorial plane was plotted as given in Fig 6, which shows that convection patterns propagate westward throughout these simulations, and the number of convection columns changes from 4 pairs to 3 pairs when $7.0 < t < 10.0$. The drift frequency becomes almost constant when $t > 11$, but the differences between the simulations are observed. To estimate the drift angular frequency at the quasi-steady state, a component of the radial velocity described as $v_r(t) \cos(3\phi - \omega t)$ was chosen. The drift angular frequency in the quasi-steady state was estimated by the phase of a wave of this velocity component, and the drift frequency plotted as a function of time in Fig.7. As given in Fig.7, the magnitude of the drift frequency is larger than that in the case by the spectral method; i.e., the convection pattern propagates rapidly in the case of GeoFEM. As given in Table 1, the magnitude of the drift frequency in a quasi-steady state is 1.13 times that for the case by the Spectral method.

4. Discussion

The simulation results by GeoFEM and spherical harmonics expansion demonstrate similar convection patterns and time variations. As seen in Table 1, however, about deviations of 10% are observed for several values in the results. The two simulations have many differences; that is, spatial resolution, radial resolution, and initial temperatures. The resolution in the radial direction may cause serious problems. In both cases, the radial resolution affects the convection patterns around both boundaries because the radial resolution is too coarse to describe the boundary layers. The error in the case by GeoFEM may be larger than that by the spherical harmonics expansion, because the radial resolution in the case by GeoFEM is

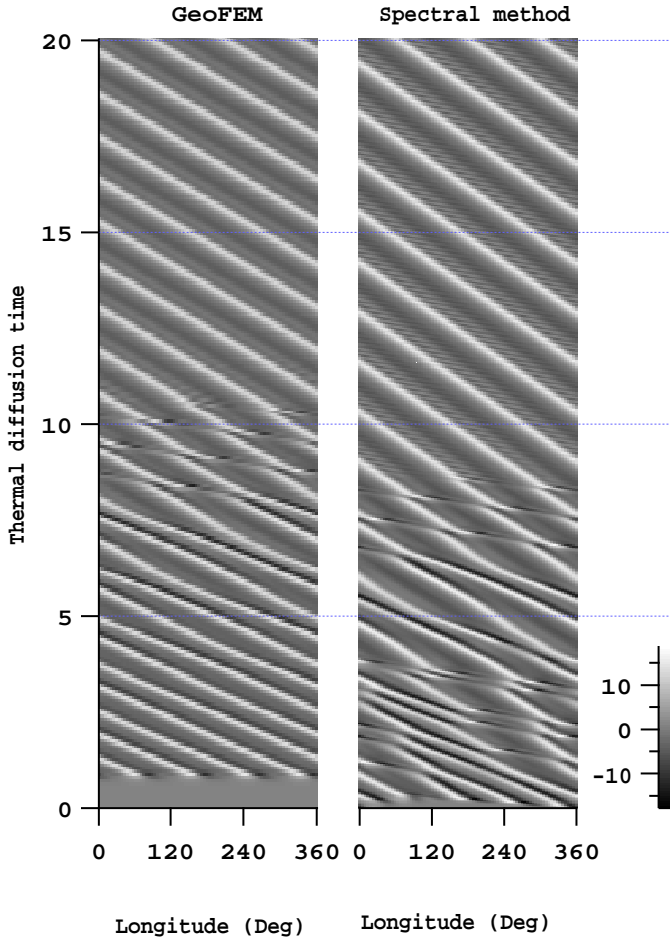


Figure 6: Radial velocity v_r along the equatorial plane and mid-depth of the shell as functions of the longitude (horizontal axis) and time (vertical axis). This figure shows the propagation of the convection pattern in the zonal direction. A positive value represents outward flows. The grayscale range is from -17.5 to 18.5.

lower than that by the spectral method. However, when a larger number of nodes are set in the radial direction, the length of the time step has to be set to a much shorter value. In fact, the simulation was performed with a grid that has 64 nodes in the radial direction and the mesh pattern was set described in Section 3. In this case, length of the time step was set to be 0.1 times the previous case, and CPU time was 20 times longer than that for the simulation given in Section 3. The simulation was executed to $t = 4.5$ and reached a quasi-steady state in a shorter period of time (see Fig.8 and Fig.9). The magnitude of averaged kinetic energy and angular momentum was 32.7 and -0.866, respectively. Only 3% difference was observed between the results by GeoFEM and the spectral method.

Therefore, the simulation was performed with a significantly higher resolution, particularly around both boundaries. This requires significantly shorter time steps. The length of time step is controlled by the diffusion terms. In order to perform simulations with significantly longer time steps, the Crank-Nicolson scheme may be more suitable scheme for solving the diffusion terms than the present scheme.

The elapsed time for the simulations shown in Section 3 is estimated as shown in table 2. It is difficult to directly compare the elapsed time by GeoFEM with that by the spectral method because of the different spatial resolutions, methods and platforms. However, it is

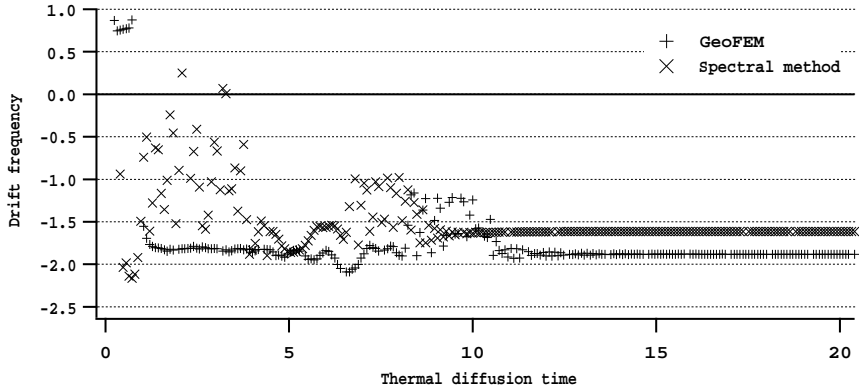


Figure 7: Drift angular frequency of the radial component of velocity with three wave numbers in the longitudinal direction at the equatorial plane and mid-depth of the shell as a function of thermal diffusion time. This plot represents the drift frequency after $t > 11$ when three pairs of convection columns are observed. A positive drift angular frequency suggests a convection pattern drift to the east.

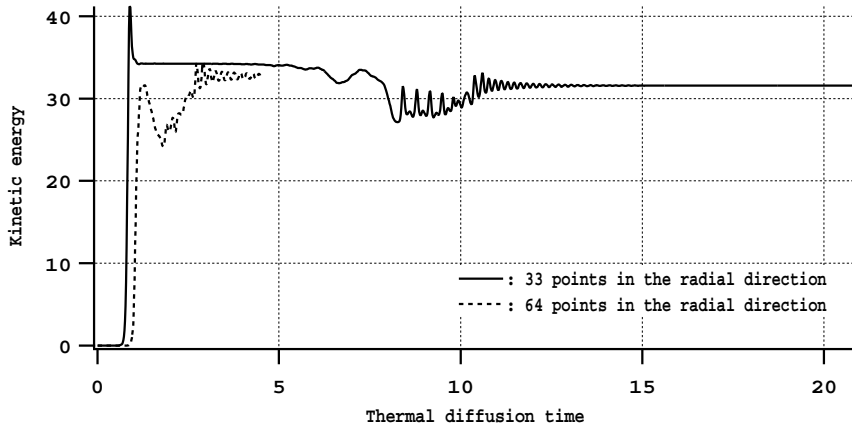


Figure 8: Time evolution of kinetic energy averaged over the spherical shell for the cases by GeoFEM. Results by the mesh with 33 layers are given by the solid line (as in Fig.5), and that by the mesh with 64 layers are given by dotted line.

noted that a MHD simulation requires time steps about that are 10 times longer than that the proposed simulations when the same parameters are set for the fluid. In this study, 2×10^5 time steps were carried out, such that it took approximately 250 hours to obtain simulation results at $t = 20.0$ and just 22 hours by the spectral method. One of reasons is that the finite element mesh had higher resolution than that used in the spectral method. The finite element mesh corresponds to a degree of truncation level of the $(3842/4)^{0.5} \sim 31$ in the spectral method. If the simulation by the spectral method is attempted with this higher degree of truncation, the process will take $(30/18)^5 = 12.8$ times the elapsed time given in Table 2. If the MHD simulation is performed with the same FEM mesh, time steps, and platform, it will take approximately 5000 hours to execute. Furthermore, because the spherical shell is divided in the radial direction in the spectral method, the simulation can not be performed on more than 64 processors. However, the proposed simulation code utilizes approximately only 4% of the peak performance of the SR8000, while approximately 30% of the peak performance is utilized in the spectral method. One of the reasons for this is that an SX-4 has SMP type vector processors. Because of the architecture of the SX-4

33 layers in the radial direction 64 layers in the radial direction

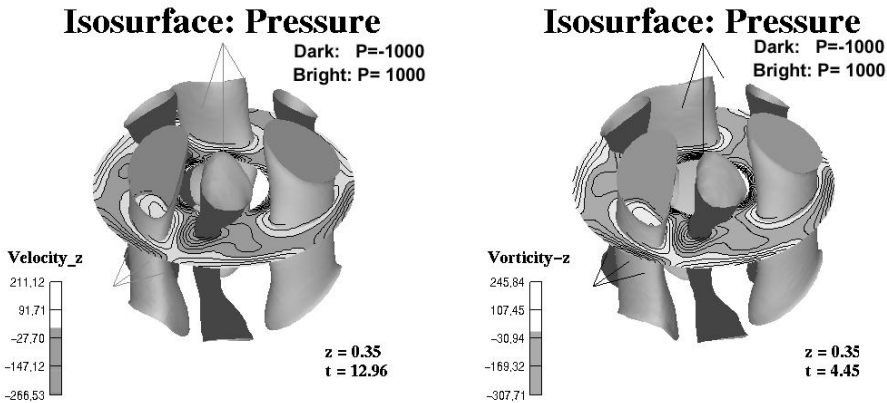


Figure 9: Convection pattern at $t = 12.96$ for the case with 33 layers in the radial direction and at $t = 4.45$ for the case with 64 layers in the radial direction. Convections are as in Fig.3.

Method	Platform	number of element	Elapsed time (sec)	Ratio (%)
GeoFEM	SR8000(8PEs)	17432	1293	4.2
GeoFEM	SR8000(16PEs)	9482	649.1	4.1
GeoFEM	SR8000(32PEs)	5449	403.7	3.7
Spectral method	SX-4(16PE)	-	33.3	31

Table 2: Elapsed times and ratio of performance to the peak performance for the first 100 time steps.

and the method of parallelization, it is easy to maximize the efficiency of the simulation. However, significant modifications are required to maximize the efficiency of the simulation. For example, the present simulation has been performed using 'flat MPI'; that is, a process for each local domain has been performed on each processor and communicates using MPI. Since one node of an SR8000 system consists of SMP type 8 processors, the simulation for each subdomain can be performed on each node. The number of domains can be decreased to 1/8 times of that in the present simulation and the number of overlapping regions can be decreased. As seen in Table 2, elapsed time is short when the number of domains is small.

The simulations were performed with just with 32 processors in the present study. However, the number of processors in each system is rapidly increasing. The Earth Simulator (ES), which is name of the supercomputer under development as part of this project, has 512 nodes with SMP type 8 vector processors. A MHD simulation based on the present simulation will be performed on the ES. Approximately 5×10^6 nodes will be set and the simulation will be performed over 10^6 steps with the Crank-Nicolson scheme for solving the diffusion terms. The advantage of the FEM approach will be clarified when the simulation is performed on a massively parallel computer such as the ES.

5. Conclusions

The authors have been developing a simulation code for the fluid motion in a rotating spherical shell modeled on the Earth's outer core to aid in the understanding of the dynamics of the fluid in the Earth's outer core. The code is based on the Thermal-Hydraulic subsystem of GeoFEM, which provides a parallel FEM platform. Simulations of thermally driven convection in the rotating spherical shell without magnetic field were performed. Tri-linear hexahedron elements were used for the spatial distribution, and the spherical shell divided into 33 layers including both boundaries. A total of 3842 nodes were set in a refined icosahedral pattern on each spherical surface. The Finite Element mesh was divided into 32 domains for parallel computation by the partitioner in GeoFEM. For time evolution of the temperature and velocity by the inertia, buoyancy, and Coriolis forces, the 2nd-order Adams-Bashforth scheme was applied. Pressure was solved by the parallel CG solver of the GeoFEM. In the simulation by the spectral method used to verify the proposed technique, poloidal and toroidal velocity components and temperature were expanded into the spectral harmonics expansion in the azimuthal and elevation direction, and the finite difference method applied in the radial direction. For the time integration, the Crank-Nicolson scheme was applied for diffusion terms and the Adams-Bashforth scheme for all other terms was applied. Because dimensionless numbers such as the Rayleigh number and the Taylor number are too large for practical implementation, they were redefined in the range appropriate for the simulation; that is, the Prandtl number was set to 1.0, the Taylor number to 2.5×10^5 , and the Rayleigh number to $1.5 \times 10^4 = 1.8R_{ac}$, where R_{ac} is the critical Rayleigh number. Rigid constrains were set on the inner and outer boundaries as a boundary condition for velocity, and the temperature set to 1 on the inner boundary and 0 on the outer boundary. Simulations were performed to 20 times the thermal diffusion time.

The convection pattern results show that three dominant pairs of convection columns that are parallel with respect to the rotation axis are formed and that these columns propagate westward in the quasi-steady state. Although different initial values of the temperature were used in the two simulation methods, similar convection characteristics were observed. However, the kinetic energy in the shell is approximately 93% that of the case using the spectral method, and the magnitude of the drift angular frequency of the convection pattern was 1.13 times larger than that for the simulation by the spectral method. These discrepancies were mainly caused by the difference in the spatial resolution in the radial direction.

It is necessary to simulate the motion of the fluid magnetohydrodynamically in order to investigate the dynamics of the Earth's core and the geodynamo process. Thus, development of a MHD code based on this subsystem is deferred to further studies. Modifications to the proposed technique are required to maximize the computational efficiency.

Acknowledgement

This study is part of the "Solid Earth Platform for Large Scale Computation" project funded by the Ministry of Education, Culture, Sports, Science and Technology, Japan through its "Special Promoting Funds of Science & Technology."

The authors would like to thank Prof. Yoshi-yuki Hayashi (Hokkaido University), Dr. Shin-ichi Takehiro (Kyushu University), and Mr. Muga Nakanishi (Tokyo Institute of Technology) for their help in understanding for the simulation results, Dr. Masaki Okada for his advice for using the Hitachi SR8000 system in the Information Science Center, National Institute of Polar Research, and colleagues in the GeoFEM project team for their support.

References

- [1] Baumgardner, J. R. and Frederickson, P. O., Icosahedral Discretization of the Two-sphere, *S.I.A.M. J. Numer. Anal.*, **22**, 1107-1115, 1985.
- [2] Bullard, E. C. and Gellman, H, Homogeneous dynamos and terrestrial magnetism, *Phil. Trans. Roy. Soc. Lond.*, **A247**, 213-278, 1954.
- [3] Busse, F. H., Thermal instabilities in rapidly rotating systems *J. Fluid Mech.*, **44**, 441-460, 1970.
- [4] Chandrasekhar, S., *Hydrodynamic and Hydromagnetic Stability*, Oxford University Press, 1961.
- [5] Christensen, U., Olson, P., and Glatzmaier, G. A., Numerical modelling of the geodynamo: a systematic parameter study, *Geophys. J. Int.* , **138**, 393-409, 1999.
- [6] Fornberg, B. and Merrill, D., Comparison of finite difference and pseudospectral methods for convective flow over a sphere, *Geophys. Res. Lett.*, , **24**, 3245-3248, 1997.
- [7] Frazer, M. C., Spherical harmonic analysis of the Navier-Stokes equation in magnetofluid dynamics, *Phys. Earth Planet Inter.*, **8**, 75-82, 1974.
- [8] GeoFEM Web Site: <http://www.geofem.org>
- [9] Glatzmaier, G. A. and Roberts, P. H., A three-dimensional self-consistent computer simulation of a geomagnetic field reversal, *Nature* , **377**, 203-209, 1995a.
- [10] Glatzmaier, G. A. and Roberts, P. H., A three-dimensional convective dynamo solution with rotating and finitely conducting inner core and mantle, *Phys. Earth Planet. Inter.* , **91**, 63-75, 1995b.
- [11] Gubbins, D. and Roberts, P. H., Magnetohydrodynamics of the Earth's Core, in *Geomagnetism* vol.2, pp.1-183, Academic Press, 1987
- [12] Honkura, Y., Iijima, T. and Matsushima, M., Magnetic field reversal resulting from a dynamo process in a spherical shell, *J. Geomag. Geoelectr.*, **44**, 931-941, 1992.
- [13] Kageyama, A., Sato, T., and the Complexity Simulation Group, Computer simulation of a magnetohydrodynamic dynamo, *Phys. Plasmas*, **2**, 1421-1431, 1995.
- [14] Kuang, W. and Bloxham, J., An Earth-like numerical dynamo model, *Nature*, **389**, 371-374, 1997.
- [15] Kuang, W. and Bloxham, J., Numerical modeling of magnetohydrodynamic convection in a rapidly rotating spherical shell: weak and strong field dynamo action, *J. Comput. Phys.*, **153**, 51-81, 1999.
- [16] Matsui, H., Studies on the Basic Processes of Magnetic Field Generation Based on MHD Simulation in the Rotating Spherical Shell, Ph.D. Thesis, Tohoku Univ., 1999.
- [17] Lesur, V. and Gubbins, D., Evaluation of fast spherical transforms for geophysical applications, *Geophys. J. International*, **139**, 547-555, 1999.
- [18] Nakajima K., and Okuda, H., Parallel Iterative Solvers with Localized ILU Preconditioning for Unstructured Grids on Workstation Cluster, *International Journal of Computational Fluid Dynamics*, **12**, 315-322, 1999.
- [19] Sakuraba, A. and Kono M., Effects of the inner core on the numerical simulation of the magnetohydrodynamic dynamo, *Phys. Earth Plant. Inter.* **111**, 105-121, 1999.

- [20] Schmalzl, J. and Hansen, U., A fully implicit model for simulating dynamo action in a Cartesian domain, *Phys. Earth Plant. Inter.* , **120**, 339-349, 2000.
- [21] Stuhne, G. R. and Peltier, W. R., Vortex Erosion and amalgamation in a New model of Large Scale Flow on the Sphere, *J. Comptational Phys.*, **128**, 58-81, 1996.
- [22] Stuhne, G. R. and Peltier W. R., New Icosahedral Grid-Point Discretizations of the Shallow Water Equations on the Sphere, *J. Comptational Phys.*, **148**, 23-58, 1999.